# Controllable Chiral Self-sorting and Guest Recognition of Ultra-stable Axially Chiral Porous Aromatic Cages

**Dongxu Cui**
Northeast Normal University
**Yun Geng**
Northeast Normal University
**Junning Kou**
Northeast Normal University
**Guogang SHAN**
Northeast Normal University https://orcid.org/0000-0002-1050-219X
**Chun-Yi Sun**
Northeast Normal University https://orcid.org/0000-0001-6060-2693
**Xinlong Wang** ( wangxl824@nenu.edu.cn )
National & Local United Engineering Laboratory for Power Battery Institution. Key Lab of Polyoxometalate Science of Ministry of Education, Northeast Normal University https://orcid.org/0000-0002-5758-6351
**Zhong-Min Su**
Northeast Normal University

**Article**

**Keywords:** ultra-stable chiral porous organic cages, chiral self-sorting, chiral sensing

**Posted Date:** August 26th, 2021

**DOI:** https://doi.org/10.21203/rs.3.rs-829250/v1



**Version of Record:** A version of this preprint was published at Nature Communications on July 11th, 2022. See the published version at https://doi.org/10.1038/s41467-022-31785-4.

# Abstract

The synthesis of ultra-stable chiral porous organic cages (POCs) and their controllable chiral self-sorting at the molecular and supramolecular level is still a daunting challenge. Herein, we report the design and synthesis of a serial of axially chiral porous aromatic cages (1-S and 1-R) with exceptional chemical stability. The theoretical and experimental studies on chiral self-sorting reveal that the exclusive self-recognition on cage formation is an enthalpy-driven process while the chiral narcissistic and social self-sorting on supramolecular assembly of racemic cages can be precisely regulated by π–π and C–H…π interactions from different solvents. Moreover, the crystallinity of 1 can be preserved under various harsh conditions including boiling water, and high-concentrated acid and alkali solutions. Further investigations on chiral sensing show that 1 possesses high enantioselectivity toward axially chiral aromatic racemates.


# Introduction

Chiral self-sorting via covalent and non-covalent bonds is a natural phenomenon, which presents a dominant ability in guiding biologic systems toward the formation of specific products out of equally multiple possibilities.[1–4] The study of external stimuli and intrinsic factors that affect chiral self-sorting in artificial systems could not only provide comprehension of recognition discipline in nature but open new opportunities for the preparation of homochiral materials and related applications for chiral sensing and asymmetric transformation.[5] Controllable processes will be helpful to acquire a deeper understanding of the principles in chiral self-sorting. Comparing with covalent and coordination bonds, the difficulty in governing the direction of intermolecular interactions makes it very hard to realize controllable chiral self-sorting. It is well known that weak molecular interactions significantly affect the supramolecular-level assembly in organisms. Therefore, it is of great significance to understand the controllable chiral self-sorting at the supramolecular level. Recently, chiral self-sorting of porous organic cages (POCs) has drawn increasing attention.[6, 7] POCs are constructed by dynamic condensation reactions and the discrete molecular cages are held together by intermolecular interactions.[8–11] Such structure feature provides a platform for the study of chiral self-sorting from covalent to weak non-covalent bonds.[8, 12–15] Researches on assembling of racemic small molecules into cages have been reported and selective chiral self-sorting has been achieved in the covalent cage formation. In spite of these, the exclusive homochiral self-sorting is quite seldom.[16–19] More significantly, the supramolecular-level chiral self-sorting on is still unexplored.

For the synthesis of chiral POCs, imine condensation has been the prevailing route, and a large number of structures have been reported, normally adopting flexible skeletons with central chiral amines as building blocks.[6, 10, 11, 20–26] Although self-correction mechanism of the reversible covalent bond greatly facilitates the accessibility of chiral POCs, the intrinsic dynamic character of imine makes this bond low-energetic stability, and prone to be attacked e.g. by nucleophiles, leading to structural decomposition even in moisture ambient humidity.[27–32] Poor chemical stability has been a thorny issue faced by chiral imine cages and restricts their practical applications.[33–35] Reduction of imine to amine have been proposed as a promising way to enhance the stability of imine cages.[36, 37] For example, via post-synthesis

modification, the imine in **CC3** is converted to amine by Cooper and co-workers, and the resultant structure can be stabilized in a wide pH range (pH = 1.7–12.3).[29] In spite of this, so far, there are quite rare imine-based POCs that can be stabilized in concentrated acids and bases, let alone pure chiral structures.[27, 36, 37] For broad applications, it is essential to build highly chemically stable chiral POCs via facile approach.

Herein, we report the one-pot synthesis of ultra-stable axially chiral porous aromatic cages (**1**-S and **1**-R) by condensation of binaphthylenediamine (BINAM) and 2,4,6-triformylphloroglucinol (TFP), and their chiral recognition. The keto-enol tautomerism induced conversion of imine bonds to amine together with the electron delocalization and the hydrophobic environment provided by the aromatic skeleton make the cage highly chemical stability in concentrated acids and alkalis for more than 1 weak. On chiral self-sorting, exclusively narcissistic self-sorting is observed in formation of the cage while the chiral self-recognition of supramolecular assembly of racemic cages can be controllably adjusted by organic solvent. Moreover, the crystalline homochiral cage and the racemic structure can reversible transformation. Notably, homochiral **1** shows appealing enantioselective recognition toward axially chiral aromatic racemates.

# Results

**Synthesis and structure analysis of chiral enantiomer of 1.** Homochiral **1**-S and -R were directly synthesized by using commercially available TFP and enantiomerically pure BINAM under solvothermal conditions. The chirality of **1**-S and -R is confirmed by circular dichroism (CD) spectra which exhibit nearly perfect mirror images in the range of 230 − 525 nm (Fig. S2). The successful condensation and the purity of product is demonstrated by $^{1}$H NMR, $^{13}$C NMR spectra (Fig. S3, S4), and mass spectrometry (observed m/z = 2330.6, calculated m/z = 2330.551) for **1**-S (Fig. S8). The disappearance of the $^{1}$H NMR signal at 12.60 and 12.57 ppm after addition of $D_2O$ confirms the presence of an exchangeable NH proton (Fig. S5), suggesting the conversion of imine bond to amine. The keto form was confirmed by $^{13}$C NMR spectroscopy (Fig. S4) in which a clear signal near 184 ppm is detected, corresponding to the carbonyl carbons.

Single-crystal X-ray diffraction (SCXRD) analysis reveals that **1**-S or -R is a [4 + 6] octahedral molecular cage composed of four TFP and six BINAM crystallizing in $F4_132$ chiral space group (Fig. 1a, 1b and Table S1). In the octahedral cage, TFP occupies four faces and is connected with naphthalene ring through C-N bonds. It is worth noting that one naphthyl of BINAM and TFP are nearly coplanar (dihedral angle: 2.558°). The lengths of C–N and C–C bond ranges from 1.365 to 1.384 Å, which are between the lengths of single (1.47–1.58 Å) and double bond (1.25–1.34 Å), indicating the formation of delocalized conjugated structures (Fig. S9).[38] This configuration leads to the dihedral angle of two adjacent planes (73.505°) slightly smaller than binaphthalene diamine monomer (79.254°). The length of C–O bonds on phloroglucinol changes from 1.43 to 1.249 Å illuminating phenolic hydroxyls are rearranged from enols into ketones.[37, 39, 42] This rearrangement makes aldehyde group more active than ordinary aromatic

aldehydes, which facilitates the condensation reaction towards C–N bond formation. The FTIR spectrum (Fig. S6, S7) of **1**-S does not show any characteristic stretching bands of imine (C = N) groups, instead, they present obvious C = C stretching around 1602 $cm^{-1}$ and C-N stretching around 1282 $cm^{-1}$. These peaks support the formation of keto–enol tautomerism. The estimated volume of the internal cavity is *ca.* 229.689 $Å^3$, calculating by VOIDOO program with 2.1 Å probe based on the crystal structure (Fig. S10).[40] These discrete octahedral cages packing in a window-to-window model generate a 3-D diamondoid porous network (Fig. 1d, 1e).

The porous nature of **1** is probed by $N_2$ adsorption. The measurements at 77 K exhibits a Type I isotherm (Fig. 4a), with a total gas uptake of 205 $cm^3/g$ at 1.0 bar and an apparent BET surface area of 343.4 $m^2/g$. Pore size distribution shows a narrow range with a pore-width of 13.9 Å (Fig. S11, S12).

**Chiral self-sorting behaviour in cage formation.** When using racemic BINAM to react with TFP, only homochiral cages are formed, as confirmed by $^1$H NMR after reaction using benzene-d6 as solvent and SCXRD signal (Fig. S14 and Fig. 3a, c). The exclusive chiral narcissistic self-sorting is not common in POCs.[17, 18, 20] According to Burnside's lemma, 11 cage isomers (including enantiomers) are possible. Eliminating the enantiomers, the possible cages are six (Fig. 2). In dynamic covalent condensation, the major products are the most thermodynamically stable or those with the lowest Gibbs free energy, in which both enthalpy and entropy have a role. In order to acquire more insight into factors for the favored formation of the homochiral cage, the enthalpy ($\Delta H$) and entropy ($\Delta S$) of all possible isomers were calculated by density functional theory (DFT) calculations (Table S2, Fig. 2). The largest energy difference of $\Delta S$ between the homochiral and heterochiral cages is only 15.11 $J•K^{-1}•mol^{-1}$ while the energy difference of $\Delta H$ reaches 150.35-311.94 kJ $mol^{-1}$ and $\Delta H$ favors the formation of a homochiral cage over the heterochiral cages. This huge energy difference leads to $\Delta G$ of homochiral cage lower than that of heterochiral ones by 102.25-316.44 kJ $mol^{-1}$. These results illuminate homochiral cage is the thermodynamically stable conformation and the exclusive chiral narcissistic self-sorting is enthalpy-driven process.

**Chiral self-sorting on supramolecular level.** The supramolecular assembly of **1**-S and **1**-R cages exhibits controllable chiral self-discrimination and self-recognition via precisely adjusting organic solvents. When the solvent is mesitylene, the racemic structure (**1**-R/S) is obtained (Fig. 3e). SCXRD analysis shows **1**-R/S crystallizes in *P*-1 space group, two enantiomer cages are stacked in wall-to-wall manners (Fig. S15), and the cavities and intermolecular space are occupied by mesitylenes. The purity of the sample is illuminated by PXRD (Fig. S16). When mesitylene is replaced with benzene or toluene, homochiral crystals without guests are obtained (Fig. 3a, c), and the structure is the same as that prepared from the enantiomerically pure precursor.

Interestingly, the homochiral and racemic crystallization presents supramolecular structural reversible transformations (Fig. 4). When equimolar crystals of **1**-S and **1**-R were dissolved in mesitylene and heated at 120°C for 3.5 days, the crystals of **1**-R/S⊃**mesitylene** were obtained as confirmed by SCXRD and PXRD

(Fig. S17). The obtained heterochiral crystals can return to homochiral crystallization in toluene under similar conditions (Fig. S17). While it has been previously reported the transformation of the crystal of homochiral cage to racemic **1**-R/S structure,[16–19] this is the first time, the controllable reversible transformation between the single crystal of homochiral and racemic structure is achieved.

DFT calculations are carried out to clarify the mechanism of solvent-controlled chiral self-sorting. Based on reduced density gradient (RDG) analysis, the intuitive information about molecular interactions for homochiral cage and racemic structure are shown in Fig. 3g and S18, S19.[41] If the neighboring cages are heterochiral, the interaction energy of the structure is only − 8.0 kcal/mol and the intermolecular distance is increased comparing with homochiral configuration. As a comparison, the interaction energy of the homochiral cage is decreased to -24.83 kcal/mol for strong π−π interactions between adjacent cages, which means the homochiral packing is more stable and preferred. When mesitylene is introduced into racemic system, the lower interaction energy of -62 kcal/mol is obtained benefiting from the π−π and C−H…π interactions between mesitylenes and cages. When the mesitylene is changed to benzene or toluene, the interaction energy is increased to -29.93 kcal/mol which is close to homochiral configuration. These conclusions well verify the experimental results and clarify intermolecular forces play an important role in cage chiral self-sorting. Besides, we find only two methyl groups at an angle of 120° can undertake the C−H…π interaction between neighboring cages while the left methyl plays a space-occupying role (Fig. S18). In order to verify the results of a theoretical calculation, three different solvents, including p-xylene, m-xylene and 5-iodo-m-xylene, were used. **1**-R/S crystal is obtained only in 5-iodo-m-xylene, and the arrangement of 5-iodo-m-xylene in the structure is similar to mesitylene (Fig. S20). Calculated interaction energy (-67.08 kcal/mol) is also similar to the case of mesitylene (-62 kcal/mol). Combining the results of theoretical calculations and experiments, the chiral self-sorting of cage can be precisely regulated through solvent and supramolecular interactions.

**Stability of 1-** S. Chemical stability is one of the knotty issues that plague the development of chiral POCs.[37] The chemical stability of homochiral **1**-S is investigated under various harsh conditions including boiling water, and concentrated base and acid (12 M NaOH, 1 M HCl and $H_2SO_4$). Excitingly, **1**-S presents outstanding stability toward water and also to both concentrated acids and bases. As confirmed by FTIR and $^1$H NMR (Fig. S21, S22,), there is not any chemical decomposition of **1**-S when it was soaked in boiling water, NaOH (12 M), HCl (1 M) and $H_2SO_4$ for 7 days. From the intact powder X-ray diffraction (PXRD, Fig. 5a) pattern and the crystal photographs (Fig. S23), we can find there is no loss of crystallinity, as well. Likewise, these treatments of concentrated acidic and basic solutions do not affect the porosity in **1**-S, as witnessed by the $N_2$ adsorption isotherms after treatment (Fig. 5b). The chemical stability of this POC towards both alkaline and acid solutions outperforms the reported POCs (Table S4). We believe the high durability of **1**-S to the extremely harsh conditions not only ascribes to the keto-enamine structure, but also benefits from the aromatic skeleton which facilitates electron delocalization and provides the steric hindrance and hydrophobicity around the amine bond preventing its hydrolysis. The high hydrophobicity of the crystal surface is verified by the water contact angle of 145.7° (Fig. S24).

In thermal stability, **1**-S also has appealing performance. Through thermogravimetric analysis (Fig. S25), it is found there is a weight loss of about 8% before 90°C, which can be attributed to the loss of solvent molecules. Then, a platform appeared before 200°C, indicating the structure can be stabilized to this temperature. In order to further prove its thermal stability, a variable temperature PXRD test was carried out with an interval of 50°C (Fig. S26). No obvious change is observed, indicated **1**-S can be stable before 200°C.

**Enantioselective recognition of biaryl molecules.** As crucial components in the biological system, the enantiomer recognition of atropisomerically biaryl molecules is of significant importance to life sciences and pharmaceutics.[43, 44] The observed supramolecular interactions may endow **1** capacity for enantioselective recognition of biaryl molecules.[45] Therefore, **1** is selected as a sensor for six enantiomers **B1-B6**. Chiral sensing experiments were conducted by immersing activated enantiopure **1** into the solution of analytes separately and evaluated by the fluorescence of analytes. To get a clear evaluation, the changes (ΔI) in luminescence intensity before and after adding **1** is normalized ($\Delta I/I_0$). As shown in Fig. 6, S27, 1-S preferred *S*-fashion substrates over the *R*-fashion, especially to **B4** with the selectivity up to 98%. Recycle experiments show the sensing ability maintains by ~ 85% after five rounds of recycling. (Fig. S28). The limit of detection (LOD) of **1**-S to S-**B4** was determined to be 0.597 $\mu$M (Fig. S29, S30). A similar selectivity also occurs in **1**-R to *R*-fashion substrates. These results demonstrate **1** could be a promising probe for recognition of enantiomer atropisomerically biaryl molecules. To clarify the internal reasons for the recognition process, molecular dynamics simulation and DFT calculations on **1**-S to R-**B4** and S-**B4** were carried out. Comparing with **1**-S/R-**B4**, **1**-S/S-**B4** has much stronger interaction energy by 16.13 kcal/mol (Fig. S31, S32 and Table S5). Moreover, larger electronic coupling for excitation energy transfer of **1**-S/S-**B4** than that of **1**-S/R-**B4** is also found (Table S5). These results suggest stronger interaction and more efficient energy transfer between **1**-S and S-**B4** may result in the observed larger changes (ΔI) in luminescence intensity.

# Discussion

In conclusion, the first pair of an axially chiral aromatic [4 + 6] POC (**1**-S and **1**-R) is constructed from the condensation of binaphthylenediamine and tridentate aldehyde. The keto-enamine structure and the steric hindrance around the amine bond, together with hydrophobic environment and electron delocalization renders **1** an exceptional chemical stability under boiling water and concentrated acid/base conditions. Controllable chiral self-sorting at both molecular and supramolecular level is observed. DFT calculations show that the exclusive self-recognition on cage formation is an enthalpy-driven process, while the narcissistic and social self-sorting on supramolecular cage assembly is regulated by different solvents *via* C–H…π and π–π interactions. The reversible transformation of homochiral cage and racemic structure is witnessed by single crystal X-ray diffraction. Moreover, **1** possesses good enantioselectivity toward a series of axially chiral aromatic racemates. This work provides new insights for the design of chiral porous aromatic cages and the related chiral self-sorting, and these robust chiral POCs may offer new prospects for the application of organic cages.

# Methods

**Synthesis of 1-**S **and 1-**R. A mixture of *S*-BINAM ([*S*]-[−]-1,1'-Binaphthyl-2,2'-diamine) or *R*-BINAM ([*R*]-[+]-1,1'-Binaphthyl-2,2'-diamine) (0.1 mmol) and 2,4,6-Triformylphloroglucinol (0.066 mmol) was dissolved in $CH_3(CH_2)_3OH$ (1 mL), toluene (5 mL) and acetic acid 6 M (0.6 mL). After stirring for 10 min at room temperature, this solution was transferred into a Parr Teflon–lined autoclave and kept at 120°C for 72 h. After cooling down to room temperature, red octahedral crystals were obtained. Yield: 42 % based on 2,4,6-Triformylphloroglucinol. Elemental analysis Calcd: C, 80.41; H, 4.12; N, 7.22. Found: C, 80.24; H, 4.30; N, 6.98.

**Synthesis of 1-**R **/** S **⊃mesitylene.** A mixture of *S*-BINAM and *R*-BINAM (1,1'-Binaphthyl-2,2'-diamine) (0.1 mmol) and 2,4,6-Triformylphloroglucinol (0.066 mmol) was dissolved in acetic acid 6M (0.6 mL), $CH_3(CH_2)_3OH$ (1 mL) and mesitylene (5 mL). After stirring for 10 min, this solution was transferred into a Parr Teflon–lined autoclave and kept at 120°C for 72 h. After cooling down to room temperature, red rod crystals were obtained and washed with $CH_3OH$. Yield: 48 % based on 2,4,6-Triformylphloroglucinol. Elemental analysis Calcd: C, 82.05; H, 5.13; N, 5.98. Found: C, 81.84; H, 5.36; N, 5.77.

**Synthesis of 1-**R **/** S **⊃5-iodo-m-xylene.** Single crystals of **1-**R/S**⊃5-iodo-m-xylene** were synthesized under the similar conditions apart from the solvent was replaced with 5-iodo-m-xylene. After slow cooling to room temperature, red rod crystals were obtained with a yield of 38 % based on 2,4,6-Triformylphloroglucinol. Elemental analysis Calcd: C, 69.54; H, 4.07; N, 5.18. Found: C, 69.81; H, 4.22; N, 4.96.

**Structural transformation from 1-**S **and 1-**R **to 1-**R/S**⊃mesitylene.** The crystalline samples of **1-**S (0.01 g) and **1-**R (0.01 g) were put in acetic acid 6M (aq) (0.6 mL), $CH_3(CH_2)_3OH$ (1 mL) and mesitylene (5 mL) in a Parr Teflon-lined stainless steel vessel and heated at 120°C for 72 h. After cooling to room temperature, red rod crystals **1-**R/S**⊃mesitylene** were obtained. Single crystal X-ray diffraction confirmed that the structure of **1-**S and **1-**R was transformed into **1-**R/S**⊃mesitylene**.

**Structural transformation from 1-**R **/** S **⊃mesitylene to 1-**S **and 1-**R. The crystalline samples of **1-**R/S**⊃mesitylene** (0.02 g) were put in acetic acid 6M (aq) (0.6 mL), $CH_3(CH_2)_3OH$ (1 mL) and toluene (5 mL) in a Parr Teflon-lined stainless steel vessel and heated at 120°C for 72 h. After cooling to room temperature, red octahedral crystals **1-**S and **1-**R were obtained. Single crystal X-ray diffraction confirmed that the structure of R/S**-ACPAC-1⊃mesitylene** was transformed into **1-**S and **1-**R.

**Chemical stability.** Cage **1** (10 mg) was soaked in 12 M NaOH, 1 M $Na_2CO_3$, 1 M HCl and $H_2SO_4$, and boiling water for 7 days. After that, the soaked crystals were filtered and washed with water (10 mL×5), ethanol (10 mL) and ether (20 mL). After vacuum drying, these samples were used for various tests, including IR, PXRD, elemental analysis, $^1$H NMR and $N_2$ adsorption. For $N_2$ adsorption, the sample (100 mg) needs to be further soaked in ether (5 mL×6, 12 h) and vacuum activation.

**Chemical sensing.** The crystal (5 mg) used for detection was placed in the standard solution ($EtOH/H_2O$, 1 mL/1 mL) of the analyte. The fluorescence spectra were recorded after 30 minutes. The excitation wavelength is 370 nm. For recycling experiment, the samples used in the first round of experiments were filtered out, and then soaked in fresh ethanol solution. Replace with fresh ethanol solvent every 15 minutes and repeat several times. The regenerated sample is placed in a fresh solution of the analyte (B4) for 30 minutes, and then the fluorescence intensity is collected. Repeat the above steps 5 times.

# Declarations


### Acknowledgement

This work was financially supported by the NSFC of China (No. 21971032, 21801038, 21771035), the Fundamental Research Funds for the Central Universities (2412019FZ007), Jilin Provincial Department of Science and Technology (No. 20190103018JH).


### Author contributions

C.Y.S. conceived the idea and designed the experiments, analyzed the results, C.Y.S. and X.L.W. co-drafted the manuscript. D.X.C. synthesized all the compounds and was in charge of structure studies and sensor experiments. Y.G. performed the DFT calculations. J. N.K. was responsible for characterization measurements including $N_2$ adsorption, PXRD. C.Y.H assisted with PXRD measurement and structure studies. G.G.S and Z.M.S. contributed to the general methodology, assisted with data interpretation and reviewed/revised the manuscript. All authors contributed to the analysis of the manuscript.

### Additional information

The authors declare no competing financial interests. Supplementary information accompanies this paper at www.nature.com/naturechemistry. Reprints and permission information is available online at http://npg.nature.com/reprintsandpermissions/. Correspondence and requests for materials should be addressed to C.Y.S. and X.L.W

### Competing financial interests

The authors declare no competing financial interests.

# References


1. Wu A, Isaacs L. Self-Sorting: The Exception or the Rule? *J. Am. Chem. Soc.* **125**, 4831–4835 (2003).
2. Jędrzejewska H, Szumna A. Making a Right or Left Choice: Chiral Self-Sorting as a Tool for the Formation of Discrete Complex Structures. *Chem. Rev.* **117**, 4863–4899 (2017).
3. Liu M, Zhang L, Wang T. Supramolecular Chirality in Self-Assembled Systems. *Chem. Rev.* **115**, 7304–7397 (2015).

4. Dong J, Liu Y, Cui Y. Supramolecular Chirality in Metal–Organic Complexes. *Acc Chem Res* **54**, 194–206 (2021).
5. Li C, Zuo Y, Zhao Y-Q, Zhang S. Chiral Self-sorting in Cage-like Compounds. *Chem. Lett.* **49**, 1356–1366 (2020).
6. Acharyya K, Mukherjee PS. Organic Imine Cages: Molecular Marriage and Applications. *Angew. Chem. Int. Ed.* **58**, 8640–8653 (2019).
7. Wagner P, *et al.* Chiral Self-sorting of Giant Cubic [8 + 12] Salicylimine Cage Compounds. *Angew. Chem. Int. Ed.* **60**, 8896–8904 (2021).
8. Sun Y, Chen C, Liu J, Stang PJ. Recent developments in the construction and applications of platinum-based metallacycles and metallacages via coordination. *Chem. Soc. Rev.* **49**, 3889–3919 (2020).
9. Rowan SJ, Cantrill SJ, Cousins GRL, Sanders JKM, Stoddart JF. Dynamic Covalent Chemistry. *Angew. Chem. Int. Ed.* **41**, 898–952 (2002).
10. Hasell T, Cooper AI. Porous organic cages: soluble, modular and molecular pores. *Nat. Rev. Mater.* **1**, 16053 (2016).
11. Mastalerz M. Porous Shape-Persistent Organic Cage Compounds of Different Size, Geometry, and Function. *Acc. Chem. Res.* **51**, 2411–2422 (2018).
12. Gong Y, Zhang Y, Qin C, Sun C, Wang X, Su Z. Bottom-Up Construction and Reversible Structural Transformation of Supramolecular Isomers based on Large Truncated Tetrahedra. *Angew. Chem. Int. Ed.* **58**, 780–784 (2019).
13. Ye Y, Cook TR, Wang S-P, Wu J, Li S, Stang PJ. Self-Assembly of Chiral Metallacycles and Metallacages from a Directionally Adaptable BINOL-Derived Donor. *J. Am. Chem. Soc.* **137**, 11896–11899 (2015).
14. Zhang J, *et al.* Asymmetric phosphoric acid–catalyzed four-component Ugi reaction. *Science* **361**, eaas8707 (2018).
15. Zhu H, *et al.* Formation of Planar Chiral Platinum Triangles via Pillar[5]arene for Circularly Polarized Luminescence. *J. Am. Chem. Soc.* **142**, 17340–17345 (2020).
16. Sisco SW, Moore JS. Homochiral Self-Sorting of BINOL Macrocycles. *Chem. Sci.* **5**, 81–85 (2014).
17. Schafer LL, Tilley TD. Efficient Diastereoselective Syntheses of Chiral Macrocycles via Zirconocene Coupling. Synthetic Control of Size and Geometry. *J. Am. Chem. Soc.* **123**, 2683–2684 (2001).
18. Beaudoin D, Rominger F, Mastalerz M. Chiral Self-Sorting of [2 + 3] Salicylimine Cage Compounds. *Angew. Chem. Int. Ed.* **56**, 1244–1248 (2017).
19. Jones JTA, *et al.* Modular and predictable assembly of porous organic molecular crystals. *Nature* **474**, 367–371 (2011).
20. Greenaway RL, Jelfs KE. High-Throughput Approaches for the Discovery of Supramolecular Organic Cages. *ChemPlusChem* **85**, 1813–1823 (2020).
21. Tozawa T, *et al.* Porous organic cages. *Nat. Mater.* **8**, 973–978 (2009).

22. Hasell T, Chong SY, Jelfs KE, Adams DJ, Cooper AI. Porous Organic Cage Nanocrystals by Solution Mixing. *J. Am. Chem. Soc.* **134**, 588–598 (2012).
23. Su K, Wang W, Du S, Ji C, Zhou M, Yuan D. Reticular Chemistry in the Construction of Porous Organic Cages. *J. Am. Chem. Soc.* **142**, 18060–18072 (2020).
24. Zhang L, *et al.* Desymmetrized Vertex Design toward a Molecular Cage with Unusual Topology. *Angew. Chem. Int. Ed.***59**, 20846–20851 (2020).
25. Jiao T, Qu H, Tong L, Cao X, Li H. A Self-Assembled Homochiral Radical Cage with Paramagnetic Behaviors. *Angew. Chem. Int. Ed.* **60**, 9852–9858 (2021).
26. Wang Y, *et al.* Elucidation of the origin of chiral amplification in discrete molecular polyhedra. *Nat. Commun.* **9**, 488 (2018).
27. Bera S, *et al.* Porosity Switching in Polymorphic Porous Organic Cages with Exceptional Chemical Stability. *Angew. Chem. Int. Ed.* **58**, 4243–4247 (2019).
28. Xu H, Gao J, Jiang D. Stable, crystalline, porous, covalent organic frameworks as a platform for chiral organocatalysts. *Nat. Chem.* **7**, 905–912 (2015).
29. Liu M, *et al.* Acid- and Base-Stable Porous Organic Cages: Shape Persistence and pH Stability via Post-synthetic "Tying" of a Flexible Amine Cage. *J. Am. Chem. Soc.* **136**, 7583–7586 (2014).
30. Swamy SI, *et al.* A Metal – Organic Framework with a Covalently Prefabricated Porous Organic Linker. *J. Am. Chem. Soc.* **132**, 12773–12775 (2010).
31. Turcani L, Greenaway RL, Jelfs KE. Machine Learning for Organic Cage Property Prediction. *Chem. Mater.* **31**, 714–727 (2019).
32. Jelfs KE, *et al.* Large Self-Assembled Chiral Organic Cages: Synthesis, Structure, and Shape Persistence. *Angew. Chem. Int. Ed.* **50**, 10653–10656 (2011).
33. Lee J-SM, Cooper AI. Advances in Conjugated Microporous Polymers. *Chem. Rev.* **120**, 2171–2214 (2020).
34. Yuan Y, Zhu G. Porous Aromatic Frameworks as a Platform for Multifunctional Applications. *ACS Cent. Sci.* **5**, 409–418 (2019).
35. Yao Z, *et al.* Dithienopicenocarbazole as the kernel module of low-energy-gap organic dyes for efficient conversion of sunlight to electricity. *Energy Environ. Sci.* **8**, 3192–3197 (2015).
36. Hu X-Y, Zhang W-S, Rominger F, Wacker I, Schröder RR, Mastalerz M. Transforming a chemically labile [2 + 3] imine cage into a robust carbamate cage. *Chem. Commun.* **53**, 8616–8619 (2017).
37. Bera S, *et al.* Odd–Even Alternation in Tautomeric Porous Organic Cages with Exceptional Chemical Stability. *Angew. Chem. Int. Ed.* **56**, 2123–2126 (2017).
38. Allen FH, Kennard O, Watson DG, Brammer L, Orpen AG, Taylor R. Tables of bond lengths determined by X-ray and neutron diffraction. Part 1. Bond lengths in organic compounds. *J. Chem. Soc., Perkin Trans. 2*, S1-S19 (1987).
39. Kieryk P, Janczak J, Panek J, Miklitz M, Lisowski J. Chiral 2 + 3 Keto-Enamine Pseudocyclophanes Derived from 1,3,5-Triformylphloroglucinol. *Org. Lett.* **18**, 12–15 (2016).

40. Kleywegt GJ, Jones TA. Detection, delineation, measurement and display of cavities in macromolecular structures. *Acta Crystallogr D* **50**, 178–185 (1994).
41. Lefebvre C, Rubez G, Khartabil H, Boisson J-C, Contreras-García J, Hénon E. Accurately extracting the signature of intermolecular interactions present in the NCI plot of the reduced density gradient versus electron density. *Phys. Chem. Chem. Phys.* **19**, 17928–17936 (2017).
42. Kandambeth S, Mallick A, Lukose B, Mane MV, Heine T, Banerjee R. Construction of Crystalline 2D Covalent Organic Frameworks with Remarkable Chemical (Acid/Base) Stability via a Combined Reversible and Irreversible Route. *J. Am. Chem. Soc.* **134**, 19524–19527 (2012).
43. Bringmann G, Price Mortimer AJ, Keller PA, Gresser MJ, Garner J, Breuning M. Atroposelective Synthesis of Axially Chiral Biaryl Compounds. *Angew. Chem. Int. Ed.* **44**, 5384–5427 (2005).
44. Hong T, *et al.* Chiral Metallacycles as Catalysts for Asymmetric Conjugate Addition of Styrylboronic Acids to α,β-Enones. *J. Am. Chem. Soc.* **142**, 10244–10249 (2020).
45. Hou Y, *et al.* Highly Emissive Perylene Diimide-Based Metallacages and Their Host–Guest Chemistry for Information Encryption. *J. Am. Chem. Soc.* **142**, 18763–18768 (2020).

# Figures

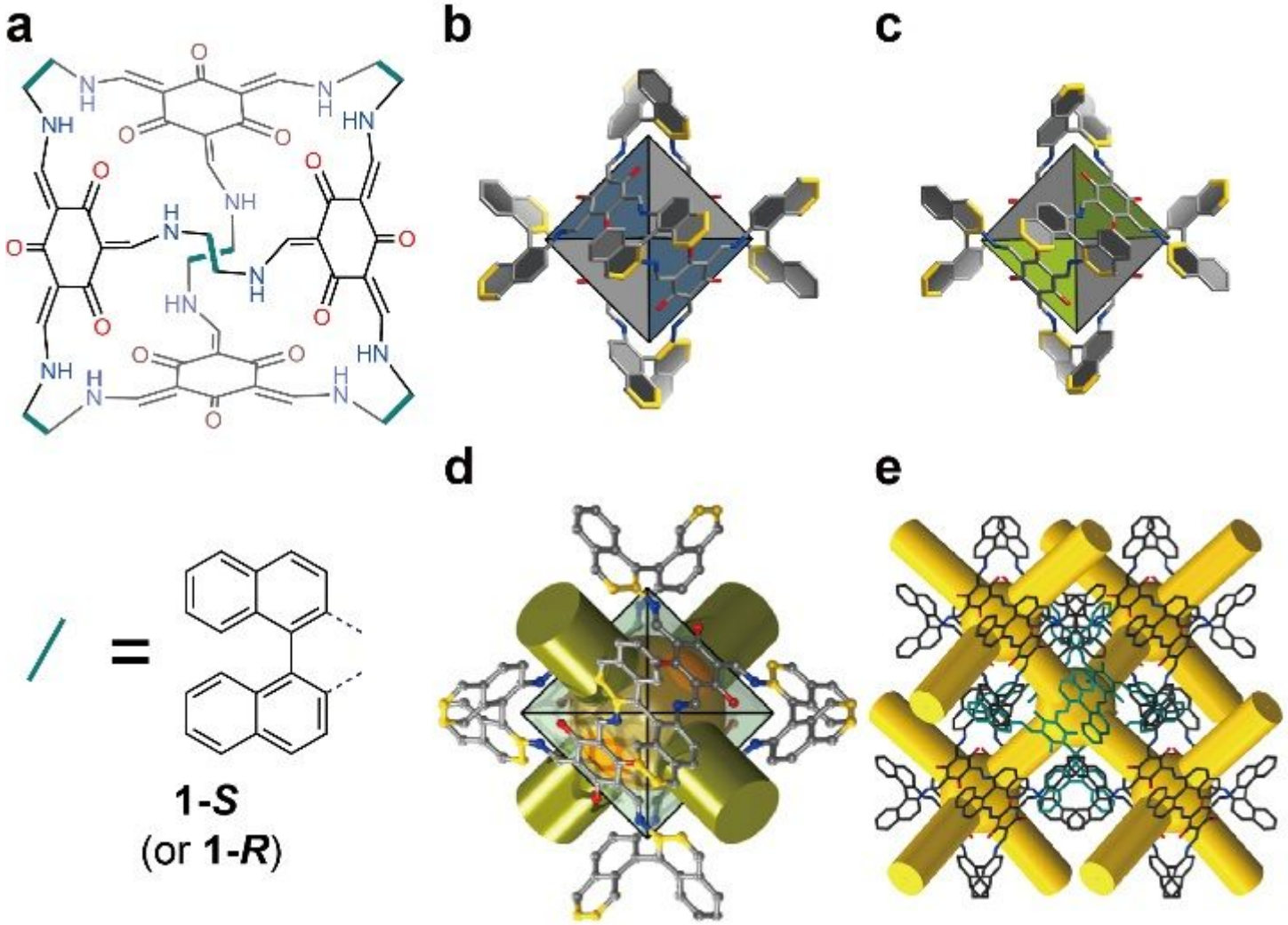


**Figure 1**

Structure of chiral enantiomer of 1. (a) Chemical structure of 1-S or 1-R. (b,c) The cage structures of 1-S and 1-R with conjugated planar in blue or green. (d) The representation of cavity and windows in 1-R. (e) The packing of 1-R with 3-D diamondoid pore network.

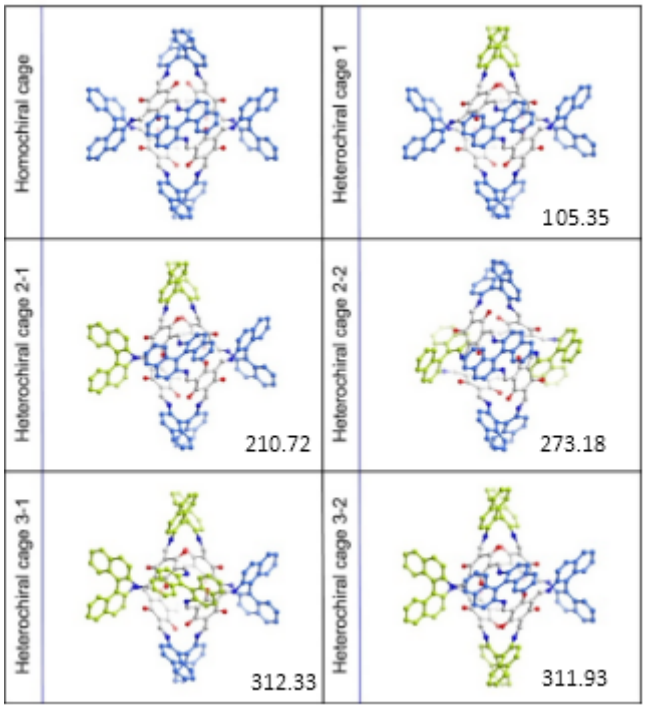


## Figure 2

The optimized cage structures based on DFT calculations. The possible cage isomers (enantiomers not included) and their corresponding enthalpies (ΔH) kJ•mol-1. blue binaphthyl: (S)-enantiomer, yellow binaphthyl: (R)-enantiomer.

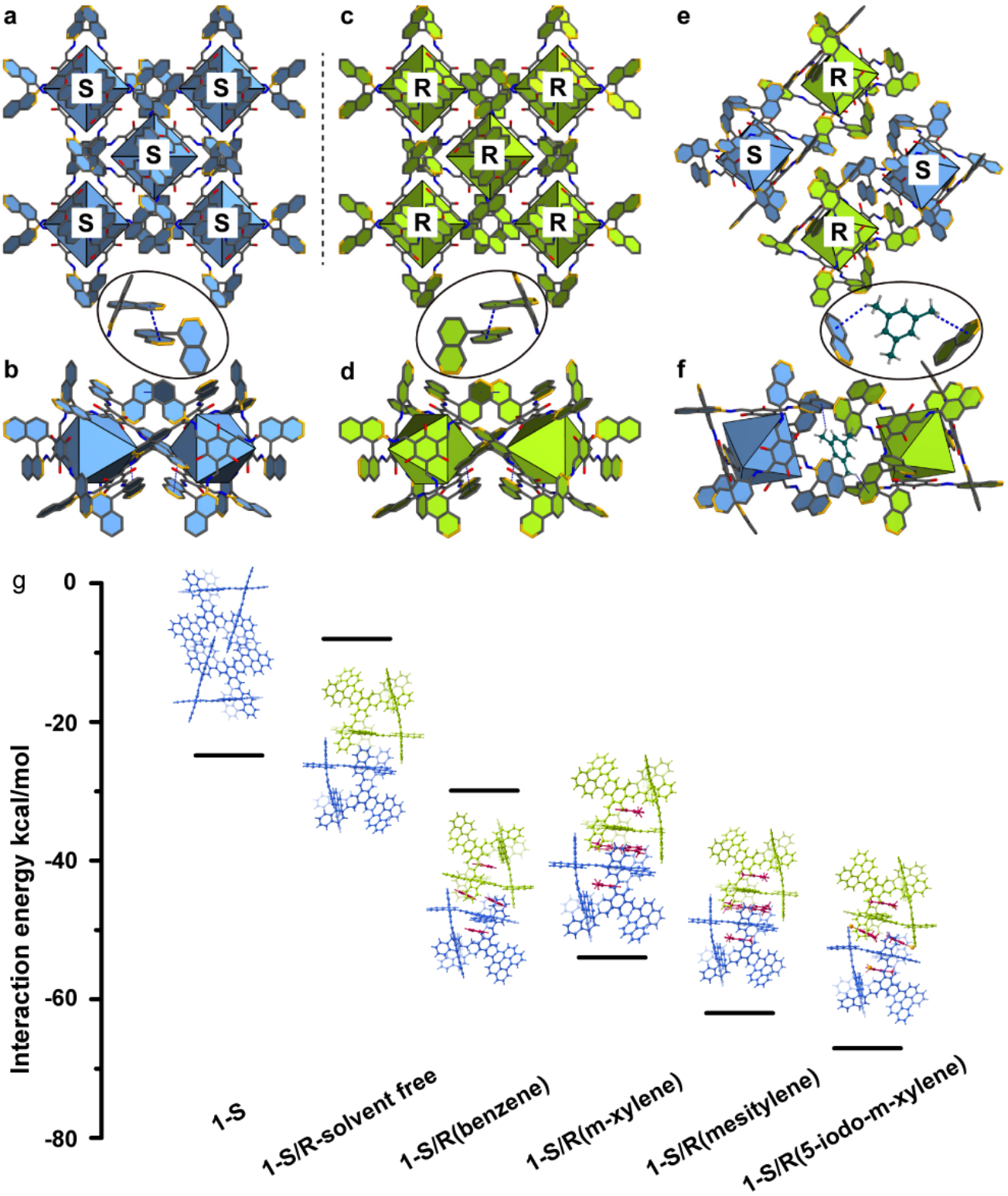


## Figure 3

The structures of cage assembly and interaction energies analysis by DFT calculations. (a-f) Schematic representation of the interaction between cages and also between solvent molecules and cages in homochiral 1 and 1-S/R crystals. (g) DFT calculated interaction energies for simulated structures.

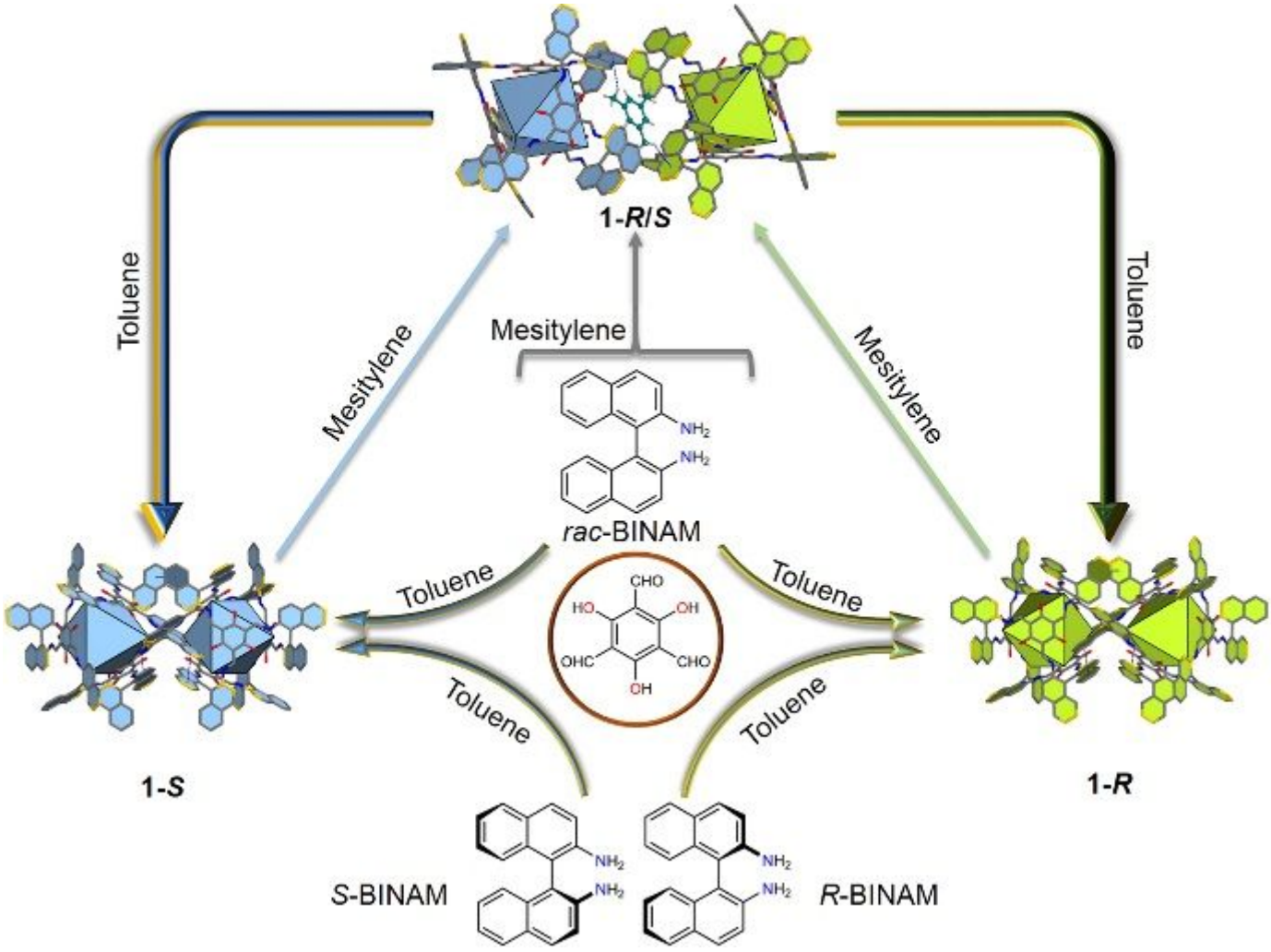


## Figure 4

Schematic illustration of the synthesis of 1 and the reversible supramolecular structural transformation between homochiral and racemic structures.

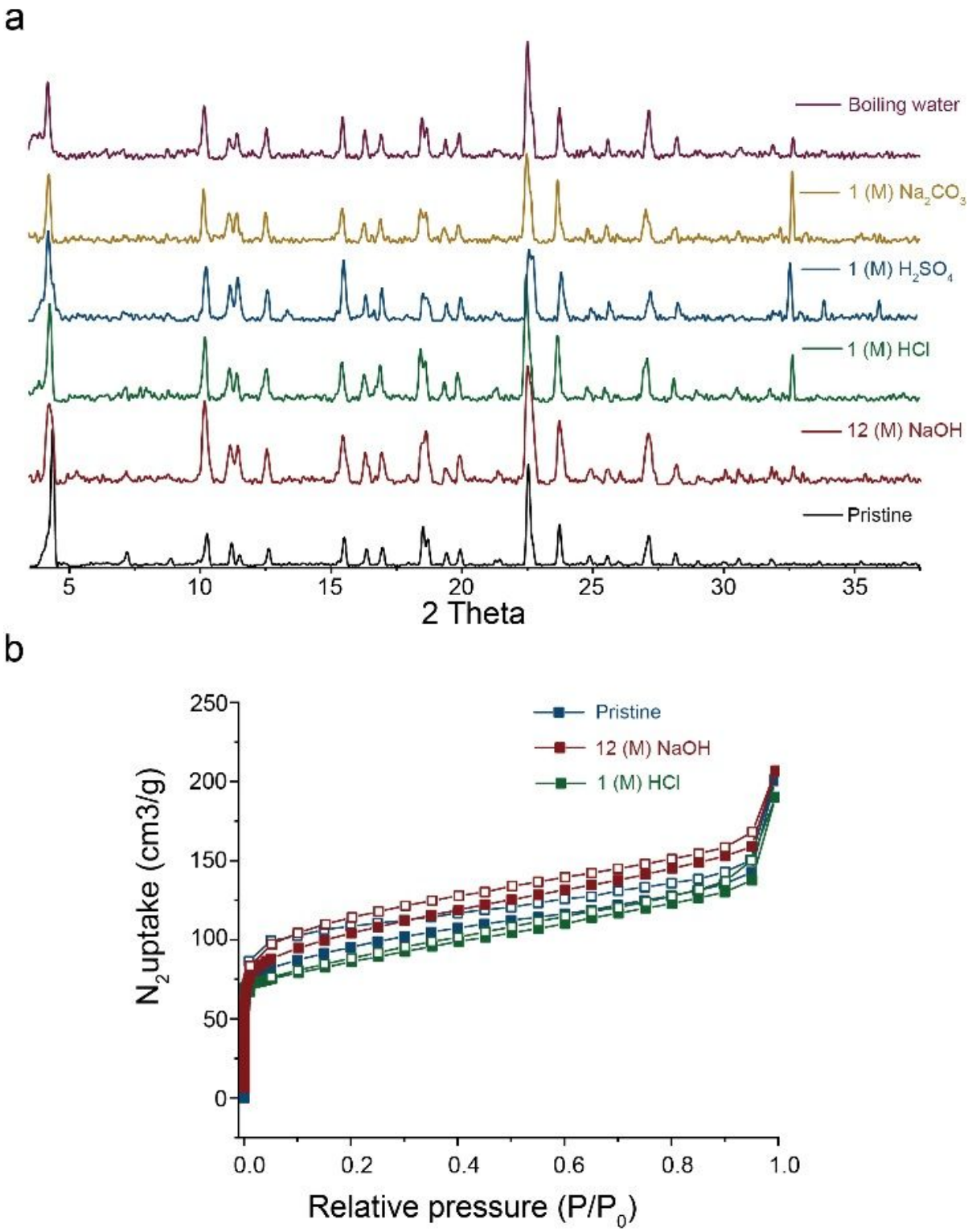


**Figure 5**

PXRD patterns and N2 sorption of 1-S under different harsh conditions. (a) PXRD patterns measured after 7 day treatment of 1-S in boiling water, 1M H2SO4, 1M HCl, 12M NaOH, and 1M Na2CO3. (b) N2 sorption of activiated 1-S and 1-S after treatment by NaOH or HCl.

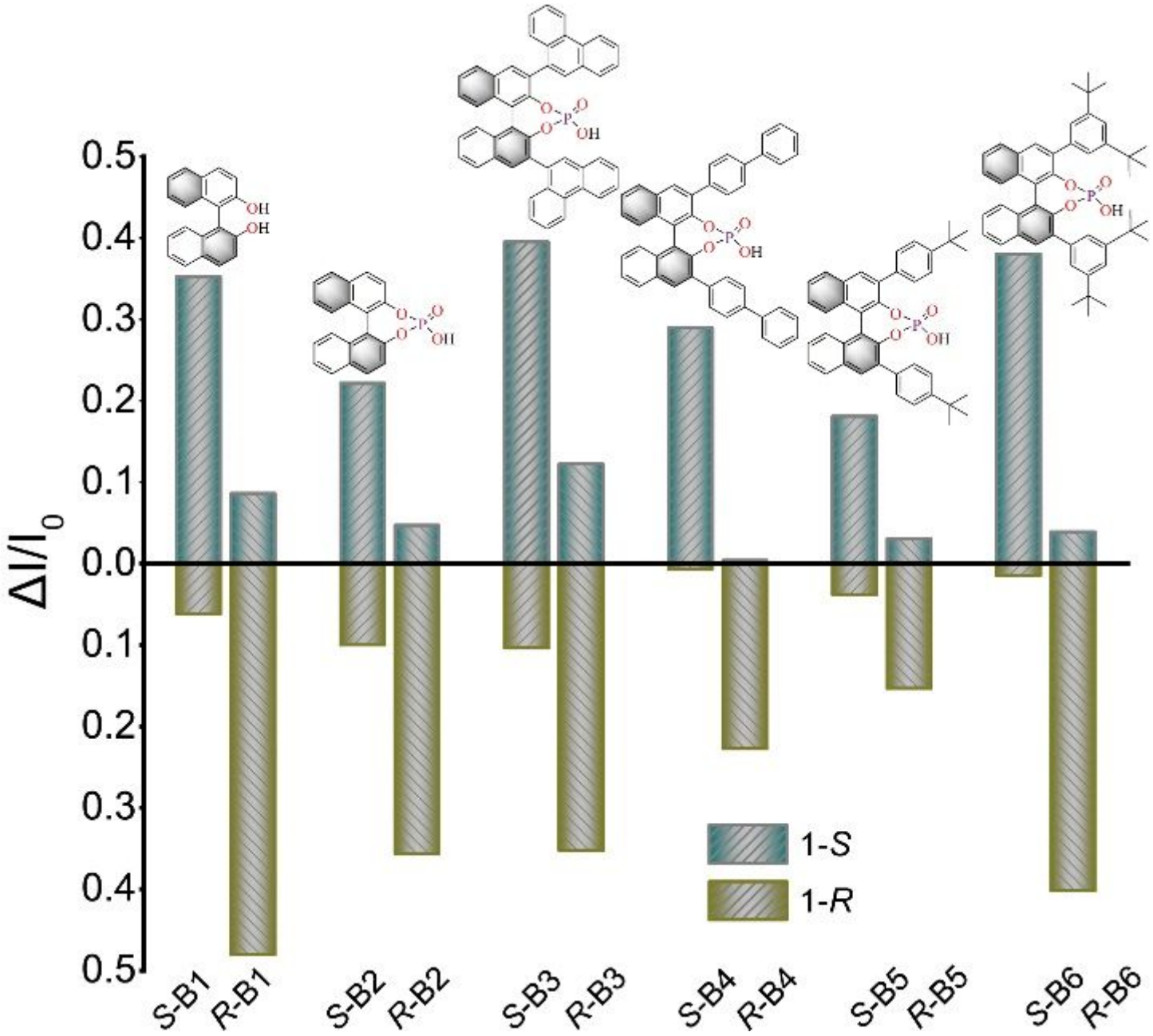


**Figure 6**

Ratio of luminescent intensity after adding 1-S (blue) or 1-R (brown) into solution of axial chiral enantiomers (B1-B6).

## Supplementary Files

This is a list of supplementary files associated with this preprint. Click to download.

- RACPAC1.cif
- RSACPAC1.mesitylene.cif
- RSACPAC1.5iodomxylene.cif

- SACPAC1.cif
- CheckCIF.pdf